Surface Science 602 (2008) 3499–3505

Contents lists available at ScienceDirect

Surface Science

journal homepage: www.elsevier.com/locate/susc

A computational study of surface diffusion of C_{60} on pentacene

R. Cantrell, P. Clancy *

School of Chemical and Biomolecular Engineering, Olin Hall, Cornell University, Ithaca, NY 14853, United States

ARTICLE INFO

Article history:
Received 21 July 2008
Accepted for publication 3 September 2008
Available online 23 September 2008

Keywords:
Anisotropy
Fullerene (C_{60})
MM3 potential
Molecular dynamics
Organic heterojunction
Pentacene
Surface diffusion and dynamics
Surface interaction energies

ABSTRACT

The morphology of the C_{60}/pentacene heterojunction is of interest for organic photovoltaic applications, yet is not well characterized. With that in mind, all-atom molecular dynamics simulation techniques were used to elucidate the diffusional behavior of small numbers of C_{60} molecules on the surface of crystalline pentacene as a probe of the molecular-level interactions between C_{60} and pentacene. The ultimate molecular probe of the pentacene surface, a single C_{60} admolecule, exhibited an anisotropic diffusion pattern that lingered in energetically preferred sites in the $[1\bar{1}0]$ direction, intercepting the (0, 1/2, 0) point in the unit cell. An Arrhenian analysis of this diffusion data gave estimates for the prefactor, D_0, and energy barrier, E_a, of 2×10^{-3} cm^2/s and 0.1 eV, respectively. Surface diffusion of one C_{60} molecule on pentacene is significantly more rapid (by about 1–2 orders of magnitude) than if even one additional C_{60} admolecule is present, implying that the C_{60}–C_{60} cohesion interaction is stronger than the C_{60}–pentacene adhesion interaction. Simulations with up to four C_{60} molecules, the practical limit of an all-atom approach, reinforced the suggestion that C_{60} likes to dewet a pentacene surface and will show a preference for forming small 3D nuclei.

1. Introduction

Organic semiconductor materials are a key component in the growing field of organic electronics, covering electronic devices such as organic light-emitting diodes (OLEDs), organic thin film transistors (OTFTs), and organic photovoltaic cells (OPVs). This paper focuses on materials for OPVs, which are of increasing interest in solar cell applications [1]. Although photovoltaics provided only 0.04% of the world's primary energy supply in 2004, their market segment has grown every year since then [2], spurred by their low cost and flexibility [3].

Simple organic solar cells can be fabricated by layering thin films of organic semiconductors between electrodes with different work functions causing electrons to flow until the Fermi levels are equal. Unfortunately, the performance of current OPVs is often hampered by poor charge transport, structural instabilities, and the low red absorption of organic materials. High photocurrent quantum efficiencies are achieved in heterojunction systems that include both electron-donating and electron-accepting layers, akin to a p–n junction in a conventional device [4]. One of the most studied of these heterojunctions for an organic/organic system involves an interface between the fullerene, C_{60}, and the small crystalline organic molecule, pentacene, with relatively large charge carrier mobilities [5].

Understanding the interfacial properties of this heterojunction and acquiring the ability to grow ordered thin films is important for improving the performance of OPVs. Even small changes in film morphology can affect charge separation at the donor/acceptor interface, hole and electron mobility, and hence overall device performance. Interactions at the buried heterojunction depend sensitively on the atomic-level structure of the materials, and are difficult to probe experimentally. This provides the motivation for a molecular-scale computational study of the properties of organic heterojunctions.

In this paper, molecular simulation is used to explore the nature of the intermolecular interactions between C_{60} and pentacene. Specifically, molecular dynamics (MD) techniques, in concert with semi-empirical interatomic potential models, are used to obtain information about surface diffusion coefficients and energy barriers. These properties are difficult to measure either experimentally or through continuum approaches.

1.1. Experimental C_{60} growth and surface diffusion simulations

There have been a number of experimental papers describing C_{60} thin film growth. Two recent papers, by Kobayashi et al. [6] and Itaka et al. [7], led to important conclusions about the order present in the C_{60} thin films. Kobayashi et al. grew C_{60} thin films on a typical dielectric layer, SiO_2, to study the influence of temperature and grain size on field-effect mobility (for OTFT applications). The C_{60} grain sizes were found to be small – at most, around 50 nm – and lacking notable orientation, which resulted in low film crystallinity. Itaka et al. improved the C_{60} crystallinity by placing an atomically flat "buffer" layer of pentacene between the C_{60} and a sapphire substrate. They claimed that the presence of the

* Corresponding author. Tel.: +1 607 255 6331; fax: +1 607 255 9166.
E-mail address: pqc1@cornell.edu (P. Clancy).

0039-6028/$ - see front matter © 2008 Elsevier B.V. All rights reserved.
doi:10.1016/j.susc.2008.09.027

pentacene layer increased the C_{60} wettability, thus improving the C_{60} film crystallinity. They observed that the C_{60} grains tend to take on a hexagonal structure. These papers show that the nature of the substrate beneath the C_{60} layer strongly influences the crystallinity of the C_{60} overlayer.

Wang et al. [8] compared the C_{60}/pentacene heterojunction to the reversed heterojunction, pentacene on C_{60}, finding much lower charge carrier mobilities in the C_{60}/pentacene case than for pentacene/C_{60}. They speculated that this is due to the difference in geometry of the two molecules, reaffirming that details of adlayer-substrate interactions play an important role in the performance of small organic molecule devices. However, there is a clear lack of fundamental understanding of the behavior of C_{60} when it interacts with the surface of pentacene. Molecular simulation is an appropriate way to begin to redress this need, showing how and why the presence of pentacene molecules affects the crystallinity of adsorbed C_{60} layers.

There are a growing number of experimental publications on the electronic properties of organic materials (e.g., charge carrier mobilities), but there has been relatively little simulation work on organic electronic materials compared to inorganic ones. There are some recent publications that use computational means to study organic electronic materials, some of which involve *ab initio* studies of idealized crystal structures of a handful of molecules (often only two molecules) reflecting interest in the electronic structure of these materials [9–11]. However, resource utilization effectively prohibits *ab initio* simulations from predicting the dynamics of surface diffusion and the structures attainable during film growth. Since film structure plays a large role in determining electronic properties, there is clearly a need to coordinate *ab initio* calculations of very small systems with semi-empirical modeling of much larger systems for which simulation of thin film growth provides a good guess at the structure of the thin film.

In that regard, there has been some recent computational effort using molecular dynamics (MD) techniques to predict surface phenomena of organic materials for a variety of applications [12–16]. Wang et al. [15] used MD to study self-diffusion mechanisms of pentaerythritol tetranitrate (PETN) on the (1 1 0) surface of crystalline PETN. They showed that PETN was stable at off-lattice sites, that it diffused along specific directions of the crystal, and that the site-to-site energy barrier was roughly 0.1 eV. As will be seen in Section 1.2, these observations of off-lattice site stability and anisotropic diffusion will also be seen in the results for the C_{60}/pentacene system studied here. A recent paper by Liu et al. [17] is one of the few dynamic simulation studies of growth processes of organic electronic materials. They combined STM experiments, coarse-grained MD, and kinetic Monte Carlo (kMC) simulations to investigate the fractal growth process of C_{60} on C_{60}. In contrast, Itaka et al. observed a hexagonal growth pattern of C_{60} on pentacene (a non-fractal growth pattern), clearly showing the effect of substrate topography on the growth pattern of C_{60}. Liu et al. found that there is a large Ehrlich–Schwöebel barrier for downward jumps of C_{60} onto C_{60}, which will help explain an observation here that will be discussed later.

1.2. Known C_{60} and pentacene structures

The equilibrium crystal structure of both pentacene and C_{60} are well known. In its bulk crystalline phase, the triclinic pentacene unit cell contains two molecules arranged in a herringbone configuration [18], with the (0 0 1) orientation as its lowest energy surface [19]. The intermolecular bonding of the pentacene molecules is a result of dipole–dipole and weak van der Waals interactions [19,20]. Pentacene is a planar molecule that is about 14 Å long and 5 Å wide. The lattice parameters of the bulk phase pentacene unit cell are a = 7.90 Å, b = 6.06 Å, and c = 16.01 Å, and the triclinic angles are $\alpha = 101.9°$, $\beta = 112.6°$, and $\gamma = 85.8°$; these values are reported by Northrup et al. [19] based on X-ray diffraction results from Campbell and Monteath Robertson [21] and were used in this paper to set up the thin films.

C_{60} is an organic molecule with 60 carbon atoms arranged in an interlocked series of 20 hexagons and 12 pentagons. At room temperature and ambient pressure, single-crystal X-ray diffraction experiments have shown that bulk C_{60} molecules prefer a rotationally disordered face-centered cubic crystal structure bound by weak van der Waals forces and having a lattice constant of 14.2 Å [22–24]. The molecular diameter of C_{60} is 7.1 Å and equilibrium center-to-center intermolecular distance is 10.0 Å [22]. C_{60} thin film lattice parameters do not vary with the lattice parameters of the substrate, in contrast to the epitaxial growth habit of most van der Waals crystals [25–28].

2. Methods

All simulations performed and reported in this paper were carried out using the freeware software package TINKER which is an atomic-scale (all-atom) modeling package with molecular dynamics (MD) capabilities for a choice of semi-empirical potentials [29]. For the MD simulations, the Beeman integration method was used to obtain positions, velocities, accelerations, and relevant system energies at each integration step (a time step of 0.5 fs). For each simulation, a short thermalization run of 5 ps was performed using a canonical ensemble in which a specified equilibrium temperature is achieved and maintained using a Berendsen thermostat [29]. Once the system reached the desired temperature without significant fluctuations (±<3 K), the simulation was continued using a microcanonical ensemble which maintains constant energy.

In order to improve the statistics of the results, simulations of all the systems reported here were repeated three times, each simulation followed for 1.5 ns with an integration step of 0.5 fs (i.e., 3,000,000 time steps). The average local pressure in the system was 10 ± 210 atm, exhibiting the typical large pressure fluctuations seen in NVE simulations. Each system of three runs was carried out at eight different temperatures between 225 and 400 K, designed to cover a range of temperatures similar to that used in experimental studies of C_{60} on the surface of pentacene [30].

Since little is known about the molecular-scale characteristics of this two-component system, we initially carried out MD simulations for all possible C_{60}–pentacene combinations of adsorbed molecules and substrate: C_{60} on the surface of pentacene (Fig. 1a), pentacene on the surface of pentacene (Fig. 1b), C_{60} on the surface of C_{60} (Fig. 1c), and pentacene on the surface of C_{60} (Fig. 1d). We began by considering the diffusion of just one adsorbent molecule on a given surface, in essence, using this adsorbed molecule as a single molecular probe of the interactions between depositing molecules and substrate. In subsequent simulations, the diffusion of up to four C_{60} molecules on a pentacene surface would be studied as a means to observe the tendency of C_{60} molecules to prefer to bind to one another rather than to pentacene.

In each case, the computational system consisted of two substrate layers with the bottom layer fixed and the top layer free to move. For the C_{60}/pentacene system, system sizes of 3×3 and 4×4 surface unit cells (in the x–y direction) were considered in order to test the effects of finite system size. A 3×3 system size involves 1356 total atoms, whereas a 4×4 system has 2364 atoms – corresponding to a large increase in computational cost. The resulting mean-squared displacements of C_{60} on pentacene showed a negligible difference between the two system sizes, implying that the 3×3 system is sufficient to properly capture the dynamics. For each of these runs, the coordinates of the center of mass of the adsorbed molecule were tracked to allow us to calculate sur-

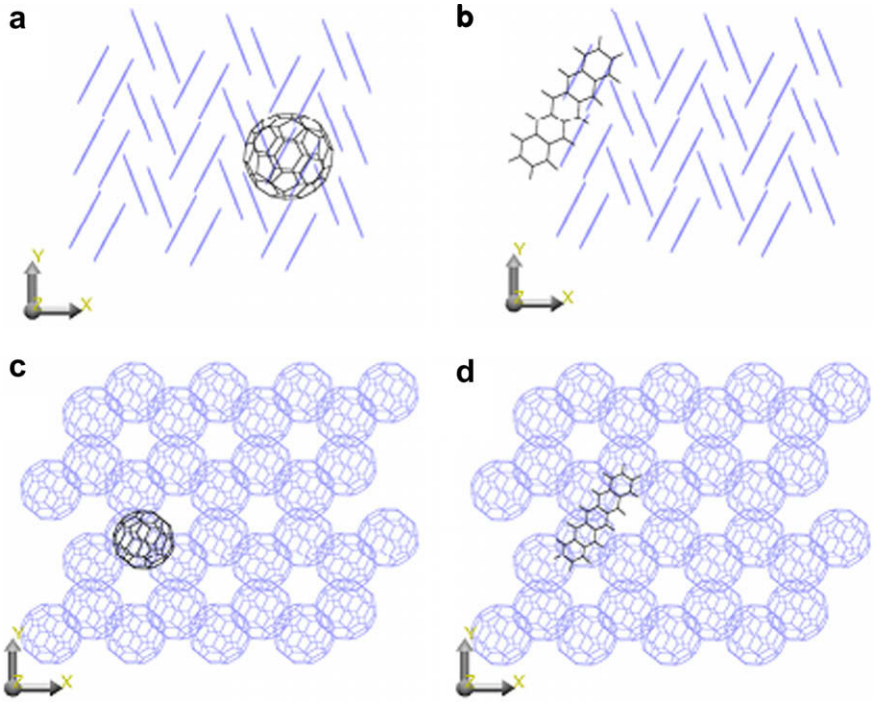

Fig. 1. Four systems considered in the MD simulations: (a) One C_{60} molecule adsorbed on a pentacene surface, (b) pentacene on pentacene, (c) C_{60} on C_{60} and (d) pentacene on C_{60}. The surface molecules are represented in a lighter color for clarity and consist of two layers in each case. Periodic boundary conditions were applied to the simulation cell in the *x*- and *y*- directions.

face diffusion coefficients, perform a site hopping energy barrier analysis, and undertake a potential energy surface mapping of the C_{60}/pentacene heterojunction using a combination of MD and static total-energy calculations.

2.1. Potential model

The most important input needed for an MD simulation is the choice of intermolecular potential model. We chose to use the semi-empirical MM3 force field since it has been shown by its developers to accurately describe hydrocarbons, namely three-, four-, five-, and six-ringed structures [31]. MM3 incorporates stretching, bending, and torsional energies as well as the van der Waals interaction energies based on atom-atom parameters related to their chemical environment [31]. Prior to our simulations, we confirmed that the MM3 model was suitable for the molecules in our system. For pentacene, we had already confirmed that the MM3 potential reproduced *ab initio*-derived MP2 intermolecular energies [32]. For the C_{60} intermolecular potential, we verified that the MM3 potential was similar to *ab initio* calculations of the C_{60}–C_{60} interactions produced by Pacheco and Prates Ramalho [33]. These *ab initio* calculations were carried out in the local density approximation to density functional theory (DFT) together with its extension for excited states, the time-dependent DFT. For comparison, the MM3 potential predicts a C_{60}–C_{60} minimum intermolecular potential of −0.34 eV at a center-to-center distance of 9.5 Å, whereas Pacheco's potential predicts −0.27 eV at 10.0 Å.

A further refinement in verifying the accuracy of the MM3-derived C_{60}–C_{60} intermolecular potential involved calculating energies for different rotational orientations of C_{60} and then averaging these energies for each center-to-center distance to see if rotational orientation affected the intermolecular energy. When two C_{60} molecules are oriented such that two apexes face each other, a larger repulsion occurs than when two planar hexagon faces face each other. Not surprisingly, the smaller the center-to-center distance, the more the spread in energy between these two orientational extremes, giving larger standard deviations to the average energies at closer distances. For example, at a distance of 8.6 Å, the C_{60}–C_{60} intermolecular potential energy is +1.1 ± 0.3 eV, and at 9.5 Å, it is −0.34 ± 0.02 eV. Overall, orientational effects appear to be small at the distances encountered in the systems considered here, which are typically greater than 9.5 Å. However, the consequence of these orientational energy differences may become important for coarse-grained simulations under conditions where molecules may approach more closely.

3. Results

3.1. Studies of a single admolecule diffusing on a surface

Fig. 2 shows the trajectories of single C_{60} molecules as each traverses the pentacene surface at different temperatures. The diffusion of C_{60} on a pentacene surface displayed considerable anisotropy which is unlike the self-diffusion trajectories of pentacene on a pentacene surface or of C_{60} on C_{60}. Fig. 3 shows a comparison of the center-of-mass trajectories of C_{60}/pentacene, pentacene/pentacene, C_{60}/C_{60}, and pentacene/C_{60} at room temperature. In cases where pentacene is the substrate, the trajectories appear to follow distinct trends (running along certain directions), whereas, in the C_{60}-as-substrate cases, there is no clear direction of diffusion. At all the temperatures tested for the C_{60}/pentacene system, there appear to be preferences for "runs" of the C_{60} admolecule, punctuated by periods of residence at certain clearly identifiable sites on the substrate's lattice. At and below room temperature, many trajectories tended to follow valleys between the pentacene rows (the $[1\bar{1}0]$ direction that intercepts the 0, 1/2, 0 point in the unit cell), which implies that the substrate topography influences the C_{60} molecule's trajectory. The fullerene molecules show a tendency to get trapped in "wells" sited between the hydrogen atoms of the top pentacene molecules, suggesting that there is a site-hopping energy barrier. As expected, the degree of anisotropic diffusion decreases with increasing temperature, as can be seen in Fig. 2. Once

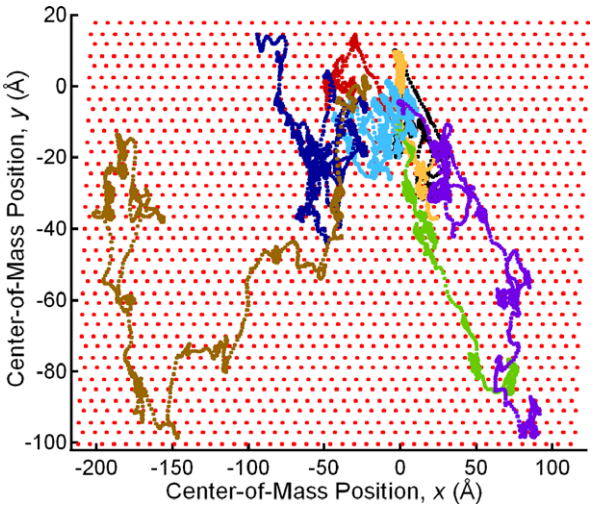

Fig. 2. Trajectories of a C_{60} molecule over the surface of pentacene taken from 1.5 ns MD simulations at temperatures from 225 to 400 K. The red dots correspond to the time-averaged positions of the top hydrogen atoms on the topmost pentacene layer of the substrate. Trajectories of C_{60} are shown in colors to represent the C_{60} center-of-mass position at 1-ps intervals at a specified temperature. The temperatures represented are 225 K (black), 250 K (maroon), 275 K (orange), 300 K (green), 325 K (light blue), 350 K (dark blue), 375 K (purple), and 400 K (brown).

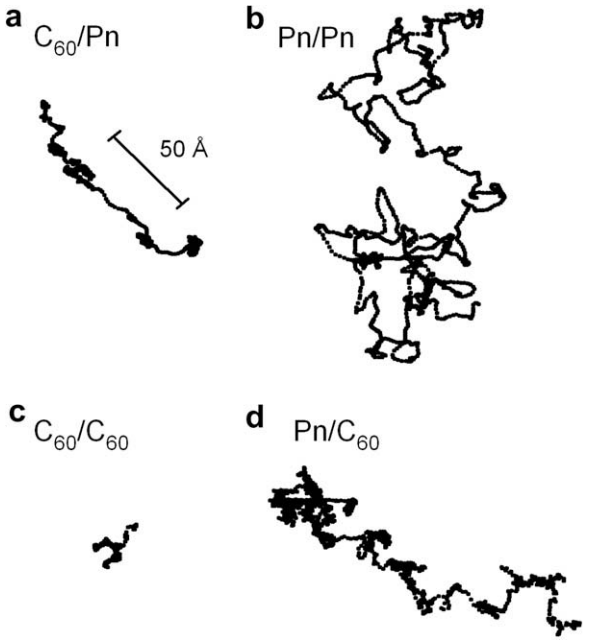

Fig. 3. Center of mass trajectories of (a) C_{60} moving on a pentacene surface, (b) pentacene moving on a pentacene surface, (c) C_{60} moving on a C_{60} surface, and (d) pentacene moving on a C_{60} surface at 300 K; each trajectory shown is over a time period of 1.5 ns.

the temperature reaches about 325 K, diffusion across the surface takes on a more random walk-like appearance.

Surface diffusion coefficients of molecules or atoms on organic surfaces are not well known. For non-organic substrates, room temperature surface diffusion coefficients of hydrogen on tungsten are on the order of 10^{-7} cm^2/s, while that of propane on silica is on the order of 10^{-3} cm^2/s [34]. As will be shown, the room temperature surface diffusion coefficient of C_{60} on the surface of pentacene falls somewhere in between these two examples. The surface diffusion coefficient, D, was obtained using the Einstein equation, $\langle l^2 \rangle = 2dDt$, where $\langle l^2 \rangle$ is the observed mean-square displacement of the diffusing admolecule, d is the dimension of the range of significant movement (2 in the case of surface diffusion), and t is time. The mean-squared displacement was measured as an ensemble average over varying time intervals (141 time origins at 100-ps intervals). Plotting $\langle l^2 \rangle$ as a function of time, t, the diffusion coefficient is found from the slope (divided by 4) at long times.

Fig. 4 shows the calculated surface diffusion coefficients as a function of temperature for the four systems shown in Fig. 1. The general trend in each case is the expected increase in diffusion coefficient with temperature. Data for the pentacene/pentacene systems appear to display greater variance in surface diffusion coefficients compared to the other systems. This is due to the larger average surface diffusion coefficient values. The coefficients of variation for the pentacene/pentacene system for all data points were less than one, indicating low variance as displayed by the other systems. The most notable trend in Fig. 4 is the roughly two orders of magnitude difference between diffusion coefficients in the pentacene/pentacene and C_{60}/pentacene systems (see Table 1). The magnitude of the diffusion coefficient is highest for pentacene on pentacene (on the order of 10^{-4} cm^2/s), followed by pentacene on C_{60} (a factor of four slower), then C_{60} on pentacene (a factor of five slower still) and, finally, C_{60} on C_{60} (nearly 2 orders of magnitude slower). At these temperatures, the diffusion coefficient for C_{60} on C_{60} is quite small, about 2.5×10^{-6} cm^2/s, which agrees with the relatively immobilized behavior of C_{60} on C_{60} shown in Fig. 3c; this seems to imply a strong interaction between C_{60} molecules.

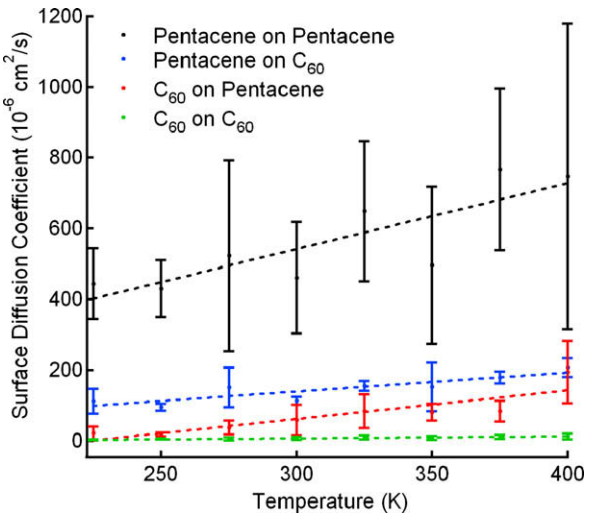

Fig. 4. Surface diffusion coefficients versus temperature averaged from several 1.5 ns MD simulations. Five pentacene/pentacene simulations were included in the averages shown; the rest were run three times. Dotted straight lines are added to guide the eye.

Table 1
Average surface diffusion coefficients for pentacene on pentacene, pentacene on C_{60}, and C_{60} on C_{60} (first three columns) compared to that for one, two, and three molecules of C_{60} diffusing over a pentacene surface (last three columns)

Temperature (K)	Average surface diffusion coefficient ($cm^2/s \times 10^{-6}$)					
	1−Pn/Pn	1−Pn/C_{60}	1−C_{60}/C_{60}	1−C_{60}/Pn	2−C_{60}/Pn	3−C_{60}/Pn
225	445	112	2	22	1	2
250	431	94	5	18	14	4
275	523	151	6	37	11	5
300	461	114	6	58	14	9
325	649	158	9	83	21	16
350	498	152	8	81	36	21
375	767	179	11	84	25	8
400	747	208	12	195	66	38

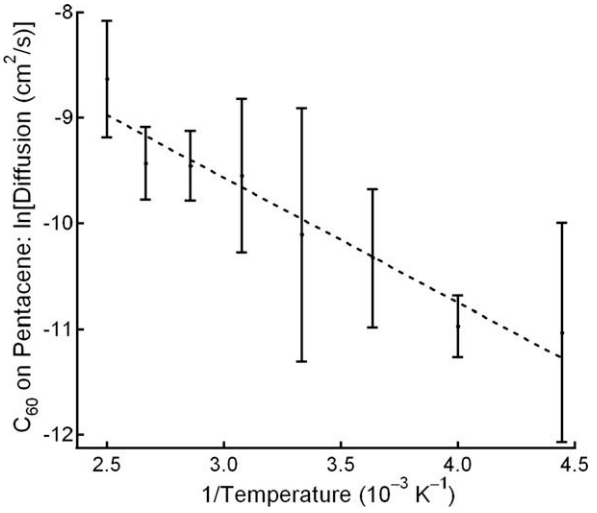

Fig. 5. Natural logarithm of the diffusion coefficient (averaged over three runs) versus inverse temperature. A linear fit to the data was used to provide estimates of the Arrhenius prefactor, D_0, and the activation energy, E_a. The dotted straight line is added to guide the eye.

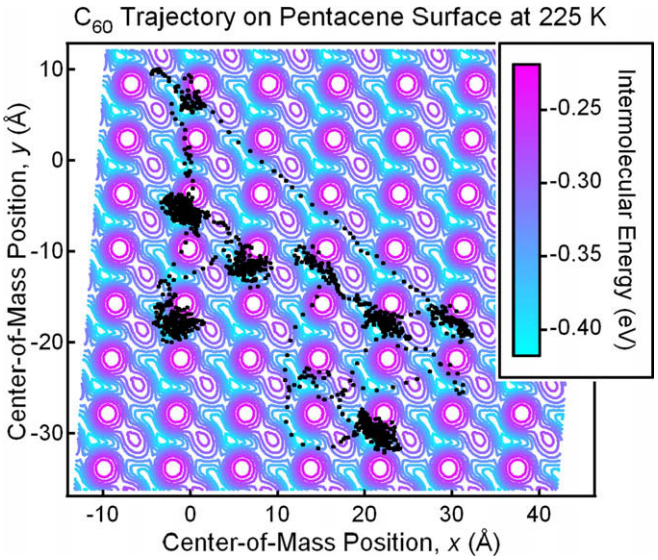

Fig. 6. Surface interaction energy between a C_{60} molecule and the pentacene surface (covering 56 unit cells) to differentiate higher energy (pink) and lower energy (aqua) regions. The energy surface is overlaid with a trajectory from an MD simulation of C_{60} on pentacene at 225 K, shown as black dots), demonstrating the close correlation between energy minima and preferred diffusion paths.

The scale of differences in diffusion coefficients for the four single-admolecule systems was unexpected, perhaps highlighting the fact that differences in admolecule shape and, ultimately, intermolecular forces strongly influence interfacial dynamics. For each substrate, the pentacene admolecule exhibited larger surface diffusion coefficients than the C_{60} admolecule. This can most likely be attributed to the differing geometry of the two molecules. The admolecule's point of contact with the surface is smaller for C_{60} than for pentacene, making it more likely for C_{60} to get trapped in troughs on the surface and have a lower surface diffusion coefficient. This is further evidenced by the C_{60} trajectories in Fig. 3a and c as compared to the pentacene trajectories in Fig. 3b and d.

Considering the temperature dependence of the observed diffusion, Fig. 5 shows the average value of the natural logarithm of the diffusion coefficient, $\ln(D)$, taken over three simulation runs. The average value appears to follow Arrhenius-like behavior, but, given fairly substantial error bars, the system cannot be unequivocally identified as such. Nonetheless, if we assume Arrhenius behavior and use a linear fit to the data shown in Fig. 5, values for the prefactor (D_0) and activation energy (E_a) in the Arrhenius equation, $D = D_0 e^{-E_a/kT}$, were found to be roughly 2×10^{-3} cm^2/s and 0.1 eV, respectively. The activation energy has about the same order of magnitude as kT at room temperature, thus it can at least be said that the systems do not behave like lattice gases.

Returning to consideration of the preference of C_{60} molecules to reside and diffuse along preferred sites on the surface of pentacene, we used a function within TINKER to map the potential energy surface for a single C_{60} molecule on pentacene (Fig. 6). Single point energy calculations were performed for 400 unique positions of the C_{60} molecule on the surface pentacene unit cell. For each point, rotational degrees of freedom of the C_{60} molecule were taken into account, minimizing the energy in the z-direction to get the most accurate average potential energy value possible. Fig. 6 shows that, per unit cell, there are two distinct minima present (the most intense aqua color) and two maxima (the most intense pink color).[1] The lowest-energy positions were not intuitively obvious. Indeed, they were difficult to predict based on the geometric positions of the top hydrogen atoms on the pentacene molecules, thus the potential energy surface provides a convenient way to determine exactly where the energy minima lie. On this surface energy map, we overlaid the trajectory of C_{60} on pentacene obtained from a typical MD run at 225 K. This confirmed that the observed "traps" for C_{60} molecules on the pentacene surface seen in the MD run correspond to low-energy locations on the surface predicted by potential energy surface and that the anisotropy coincides with patterns in the contours. Depending on the energy well to which the C_{60} would "jump," the saddle point energy barrier ranges from 0.02 eV ($\sim kT$ at room temperature) to 0.12 eV, which agrees with the order-of-magnitude estimate of E_a = 0.1 eV made by the Arrhenius analysis obtained from Fig. 4.

In order to determine how often the C_{60} molecule encounters these energy barriers, it is necessary to consider the kinetic energy relative to the energy barriers. If the kinetic energy is much larger than the energy barriers, the C_{60} admolecule will exhibit Brownian-like motion; if the kinetic energy is smaller than the energy barriers, the C_{60} admolecule will exhibit activated site-to-site hopping. Fig. 7a shows the total kinetic energy of the C_{60} admolecule at 225 K and 400 K as a function of simulation time. The kinetic energy was calculated post-simulation by the sum of translational and rotational kinetic energies and assumes the C_{60} to be a perfect rigid-body sphere. Fig. 7b shows the four different saddle point energy barriers (black lines) and the largest possible energy barrier (red line) on the surface of pentacene. It should be noted that the fluctuations in the kinetic energy are probably due to an exchange of energy between the C_{60} admolecule and the pentacene substrate. At 225 K, the molecule can invariably overcome the energy barrier along path 1 (shown in Fig. 7b), which resembles a valley. It can often travel along paths 2 and 3, less often along path 4, and rarely over the largest possible energy barrier. Looking at the effect of temperature, the C_{60} molecule at 225 K spends about 70% of its time with kinetic energy below the saddle point barrier 3 (confining it in the valley) whereas, at 400 K, it only spends about 40% of its time confined in the valley. Correspondingly, the 225 K trajectory (black dots in Figs. 2 and 6) exhibits motion akin to what has been described as a "sub-diffusive" process [35], where the adsorbed molecule seems immobilized in certain sites, occasionally hopping to the next one. In contrast, the 400 K trajectory (brown dots in Fig. 2) resembles Brownian motion with little or no energy barrier to retard the motion of the adsorbed molecule. It is possible

[1] For interpretation of the references to color in Figs. 2, 6, and 7, the reader is referred to the web version of this article.

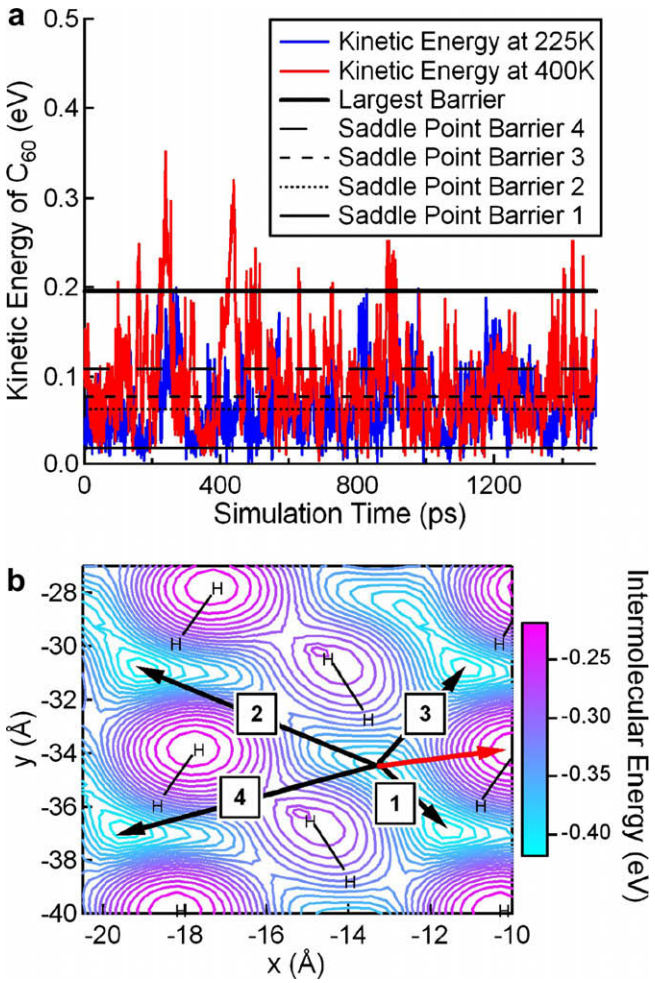

Fig. 7. (a) Kinetic energies of the C_{60} admolecule at 225K and 400K compared to energy barriers along specific directions. (b) Directions of the four saddle point energy barriers (black lines) and the largest energy barrier (red line) overlaid on the surface interaction energy of C_{60}/pentacene.

that in the limit of longer timescales than are accessible by molecular dynamics, this sub-diffusive behavior would disappear, replaced by random walk-like diffusion. This is beyond our capability to address with this approach, but we are attempting to explore this issue with a combination of MD and kMC approaches.

Up to this point, only single admolecules have been considered in order to allow admolecule-substrate interactions to be investigated independent of admolecule–admolecule interactions. From these single admolecule studies, we found that C_{60} diffuses anisotropically in the $[1\bar{1}0]$ direction, the C_{60}/pentacene surface diffusion coefficients are on the order of 10^{-5} cm^2/s at experimentally relevant temperatures (significantly smaller than pentacene/pentacene diffusion coefficients, on the order of 10^{-4} cm^2/s), and there are site-to-site energy barriers of about 0.1 eV on the pentacene surface. These findings are relevant for a C_{60} coverage situation where C_{60} molecules do not interact with one another, but it should be noted that this is not necessarily the case of low coverage. For example, at low coverage one could have small clusters of C_{60} interacting with one another.

3.2. Studies of multiple admolecules on a surface

Consideration of larger systems, involving 1–3 additional admolecules of C_{60}, greatly enlarges the total number of atoms in the system because as the number of admolecules increases, the system size has to be scaled appropriately larger to prevent unwanted interactions between C_{60} molecules and their periodic images. The largest system studied here involved four C_{60} admolecules, leading to a system containing 7296 atoms. Observation of the C_{60}–C_{60} intermolecular potential energy given by the MM3 model shows that the equilibrium center-to-center distance is 9.5 Å at the potential energy well of −0.34 eV and the range of the potential, the distance beyond which the intermolecular potential is essentially zero, is approximately 12 Å. Thus a system containing two C_{60} molecules adsorbed on pentacene will require a computational cell at least 24 Å in length (twice the range of the potential) on the shortest edge of the x–y surface of pentacene.

The behavior of two, three, and four C_{60} molecules adsorbed on a pentacene surface was considered in order to investigate the tendency of C_{60} to "wet" the pentacene surface at higher coverage conditions. Due to the larger numbers of atoms in these systems, the computational cost increased significantly relative to a single C_{60} admolecule; a single MD simulation of two and three C_{60} molecules on a pentacene surface for 1.5 ns took approximately 2 and 3 weeks, respectively, on an AMD Opteron with a 2.6 GHz CPU (or 1.5–2 weeks on an Intel Xeon 3.16 GHz CPU). Simulations containing 2- and 3-adsorbed molecules started out with C_{60} molecules located at random positions on the surface. In all cases, once a C_{60} molecule came within the range of the intermolecular potential of any other C_{60} molecule, they remained in contact. This was true even at the highest temperature tested, 400 K. Two adsorbed molecules formed a dimer, roughly 10 Å apart, once they were in contact with one another. For the 3-admolecule case, the C_{60} molecules formed a roughly equilateral triangle on the surface when they came in close enough contact, and they stayed that way for the remainder of the simulation. We have no evidence of molecules breaking away from the clusters over the relatively limited 1.5-ns timeframe of the simulations.

Surface diffusion coefficients were calculated for each C_{60} molecule in systems containing one to three adsorbed C_{60} molecules on pentacene as a function of temperature. Fig. 8 shows that there is a slight increase in the surface diffusion coefficients with temperature for systems containing one to three adsorbed C_{60}

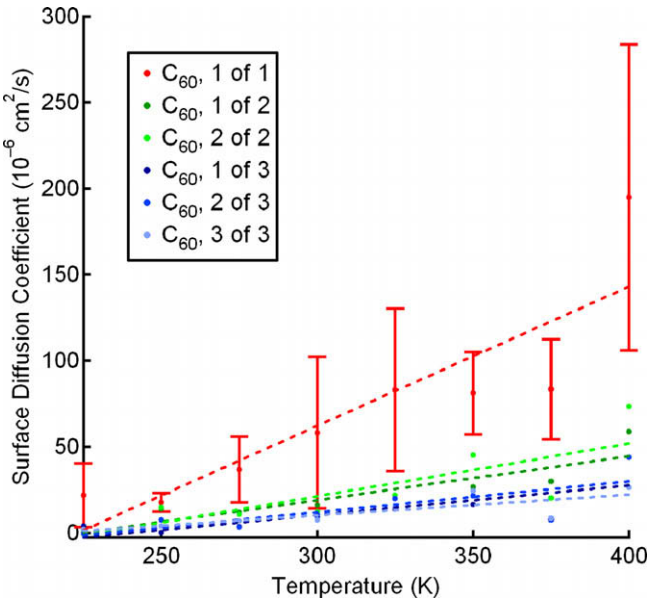

Fig. 8. Surface diffusion coefficients of multiple C_{60} molecules versus temperature. The system containing one C_{60} molecule was run three times (shown also in Fig. 4); the two- and three-C_{60} molecule systems were run only once.

molecules. There is a significant decrease in the surface diffusion coefficients when going from one to two adsorbed C_{60} molecules on the surface, with a smaller decrease when a third C_{60} molecule is adsorbed in the vicinity. This evidence, in conjunction with the data shown in Fig. 3a and c, implies that C_{60}–C_{60} cohesion is stronger than the adhesion of C_{60} on pentacene.

One simulation was performed where a fourth C_{60} molecule was placed on top of three adsorbed C_{60} molecules at the start of the simulation so as to form a pyramid. The goal of this run was to determine the tendency of the fourth C_{60} molecule to roll over the edge of the C_{60} island and adsorb directly on the pentacene surface. For the short length of the simulation, 1.5 ns, the fourth C_{60} molecule showed no tendency to leave its position atop the other C_{60} molecules. Since this simulation took a long time to finish (more than 3 weeks), it was not practical to pursue the simulation of larger systems. A simulation run of a similar duration for pentacene on pentacene was long enough for the pentacene molecule on top of the tiny island to jump down onto the terrace below.

4. Conclusions

From fully atomistic MD simulations, we found interesting results for the diffusion of C_{60} molecules on a surface of crystalline pentacene. A single C_{60} molecule exhibits an anisotropic diffusion pattern in the valleys between topmost pentacene hydrogen atoms, pausing near preferred low energy sites between the topmost pentacene hydrogen atoms. This diffusion behavior is very similar to previous MD simulation work by Wang et al. for a different organic molecule (PETN diffusing on crystalline PETN). The Arrhenius analysis of one C_{60} molecule diffusing on pentacene yielded estimates of the Arrhenian pre-factor, D_0, and the site-to-site energy barrier, $E_a - 2 \times 10^{-3}\,cm^2/s$ and 0.1 eV, respectively. Although there are considerable error bars on these values, the Arrhenian estimate of E_a agreed well with the site-to-site energy barrier found on the contour energy plot of about 0.1 eV (Fig. 6b). The existence of these regularly arranged preferred sites suggests that near-epitaxial growth of C_{60} can be made on a pentacene surface. The kinetic energy of C_{60} at different temperatures compared to the different anisotropic energy barriers on the pentacene surface further proved that anisotropy occurs below room temperature when the C_{60} molecule rarely has the necessary kinetic energy to overcome the valley-to-valley energy barrier. The directionality in the energy barriers, shown in Fig. 6b, suggests that thin film growth of C_{60} could be well captured by a lattice kMC approach, which we are currently pursuing.

At room temperature, the addition of more C_{60} molecules on the surface of crystalline pentacene, causes the average C_{60} diffusion coefficient to decrease by a factor of four when even one more C_{60} molecule is nearby. This decrease continues as a third C_{60} molecule is placed near the other two. This clear preference for C_{60} to reside close to other C_{60} molecules shows that C_{60}–C_{60} cohesion is stronger than C_{60}–pentacene adhesion. It also implies that the deposition of C_{60} on pentacene is likely to result in the growth of small 3D nuclei. Further support for the tendency of C_{60} to dewet a pentacene surface was provided by the fact that a C_{60} molecule placed on top of a small 3-molecule island of C_{60} (a site where it interacted only with other C_{60} molecules) showed no tendency to jump down from the island and interact either with the pentacene surface or the C_{60} island edges in contrast to a similar pentacene island. Although our simulation runs are relatively short, this result is confirmed by the results of Liu et al., who found that there is a considerable Ehrlich–Schwöebel barrier for downward jumps of C_{60} onto a C_{60} surface.

The relatively large system sizes and intermolecular complexity of the models used here are such that we have essentially reached the limits of system size that can be studied using serial computing. Studying more than five admolecules of C_{60} on pentacene would be prohibitively expensive for reasonable simulation run times given that the surface has to be significantly enlarged as each additional molecule is added. A massively parallel all-atom MD simulation could, of course, ameliorate this situation; however, the existence of simple C_{60}–C_{60} potential models (e.g., the Pacheco potential model) and our observation that rotational effects are negligible beyond center-to-center distances of about 9.5 Å, suggests that it should be possible to coarse-grain the representation of the C_{60} molecules without sacrificing too much accuracy. This will allow the study of systems that are orders of magnitude larger than the ones reported here and help bridge our results to mesoscopic length- and time-scales for comparison to experiments.

Acknowledgements

We would like to thank Daniel Dougherty and Steven Robey for useful communications about their experimental findings. R. Cantrell is grateful for the financial support of an NSF IGERT Fellowship administered through the Cornell Center for Materials Research, an NSF-funded MRSEC. Finally, Intel is thanked for the provision of computing resources to the School of Chemical and Biomolecular Engineering at Cornell.

References

[1] J. Drechsel, B. Männig, F. Kozlowski, M. Pfeiffer, K. Leo, Appl. Phys. Lett. 86 (2005) 244102.
[2] OECD, IEA (2007-Jan). Renewables in Global Energy Supply – An IEA Fact Sheet. IEA. Retrieved on 2007-12-29.
[3] C.J. Brabec, Sol. Energy Mater. Sol. Cells 83 (2004) 273.
[4] J. Nelson, Curr. Opin. Solid State Mater. Sci. 6 (2002) 87.
[5] J. Wang, H. Wang, X. Yan, H. Huang, D. Jin, J. Shi, Y. Tang, D. Yan, Adv. Funct. Mater. 16 (2006) 824.
[6] S. Kobayashi, T. Takenobu, S. Mori, A. Fujiwara, Y. Iwasa, Appl. Phys. Lett. 82 (2003) 4581.
[7] K. Itaka, M. Yamashiro, J. Yamaguchi, M. Haemori, S. Yaginuma, Y. Matsumoto, M. Kondo, H. Koinuma, Adv. Mater. 18 (2006) 1713.
[8] S.D. Wang, K. Kanai, Y. Ouchi, K. Seki, Org. Electron. 7 (2006) 457.
[9] X. Zhang, W. He, A. Zhao, H. Li, L. Chen, W.W. Pai, J. Hou, M.M.T. Loy, J. Yang, X. Xiao, Phys. Rev. B 75 (2007) 235444.
[10] G.C. Liang, A.W. Ghosh, Phys. Rev. Lett. 95 (2005) 076403.
[11] J.Y. Lee, M.H. Kang, Surf. Sci. 602 (2008) 1408.
[12] J.N. Glosli, G.M. McClelland, Phys. Rev. Lett. 70 (1993) 1960.
[13] D. Huang, Y. Chen, J. Chem. Phys. 101 (1994) 11021.
[14] Q.H. Zeng, A.B. Yu, G.Q. Lu, R.K. Standish, Chem. Mater. 15 (2003) 4732.
[15] J. Wang, T. Golfinopoulos, R.H. Gee, H. Huang, Appl. Phys. Lett. 90 (2007) 101906.
[16] M.J. Connolly, M.W. Roth, P.A. Gray, C. Wexler, Langmuir 24 (2008) 3228.
[17] H. Liu, Z. Lin, L. Zhigilei, P. Reinke, J. Phys. Chem. C 112 (2008) 4687.
[18] E.A. Silinsh, Organic Molecular Crystals: Their Electronic States, Springer-Verlag, Berlin, 1980.
[19] J.E. Northrup, M.L. Tiago, S.G. Louie, Phys. Rev. B 66 (2002) 121404.
[20] R. Ruiz, D. Choudhary, B. Nickel, T. Toccoli, K.-C. Chang, A.C. Mayer, P. Clancy, J.M. Blakely, R.L. Headrick, S. Iannotta, G.G. Malliaras, Chem. Mater. 16 (2004) 4497.
[21] R.B. Campbell, J. Monteath Robertson, Acta Cryst. 15 (1962) 289.
[22] P.A. Heiney, J.E. Fischer, A.R. McGhie, W.J. Romanow, A.M. Denenstein Jr., J.P. MacCauley, A.B. Smith, D.E. Cox, Phys. Rev. Lett. 66 (1991) 2911.
[23] A.T. Pugachev, N.P. Churakova, N.I. Gorbenko, H. Saadly, A.A. Solodovnik, Low Temp. Phys. 25 (1999) 220.
[24] K. Tanigaki, S. Kuroshima, T.W. Ebbesen, Thin Solid Films 257 (1995) 154.
[25] M. Hara, H. Sasabe, Y. Yamada, A.F. Garito, Jpn. J. Appl. Phys. 28 (1989) L306.
[26] K. Tanigaki, T.W. Ebbesen, S. Kuroshima, J. Cryst. Growth 114 (1991) 3.
[27] K. Tanigaki, S. Kuroshima, T.W. Ebbesen, T. Ichihashi, Mol. Cryst. Liq. Cryst. Sci. Technol. B 2 (1992) 179.
[28] H. Tada, K. Saiki, A. Koma, Jpn. J. Appl. Phys. 30 (1991) L306.
[29] Tinker: Software Tools for Molecular Design, 2004. <http://dasher.wustl.edu/tinker/>.
[30] E. Kuwahara, Y. Kubozono, T. Hosokawa, T. Nagano, K. Masunari, A. Fujiwara, Appl. Phys. Lett. 85 (2004) 4765.
[31] N.L. Allinger, Y.H. Yuh, J.H. Lii, J. Am. Chem. Soc. 111 (1989) 8551.
[32] J.E. Goose, P. Clancy, J. Phys. Chem. C 111 (2007) 15653.
[33] J.M. Pacheco, J.P. Prates Ramalho, Phys. Rev. Lett. 79 (1997) 3873.
[34] E.L. Cussler, Diffusion: Mass Transfer in Fluid Systems, Cambridge University Press, Cambridge, UK, 1997.
[35] R. Metzler, J. Klafter, J. Phys. A: Math. Gen. 37 (2004) R161.